

Characterization of the clock laser and spectroscopy of the $^3P_1 \leftrightarrow ^1S_0$ clock transition in ^{24}Mg

Bachelor thesis

Authors: Bjarke Takashi Røjle Christensen and Heidi Lundgaard Sørensen

Supervisors: Anders Brusich and Jan Westenkær Thomsen

Date: 28 May 2010

Abstract

The field of optical atomic clocks is of great scientific interest, as the stability and accuracy of the atomic clocks are significantly greater in the optical spectrum than in the microwave spectrum. To achieve high stability it is important to stabilize the frequency of the clock laser and characterize it as well as the transition line width of the reference atoms. In this thesis the clock laser and the reference atoms of the ^{24}Mg atomic clock setup, at the laser group at the Niels Bohr Institute at the University of Copenhagen, has been characterized.

The master laser line width was determined to be in the kilohertz regime by two different methods. First by analyzing the Pound-Drever-Hall error signal, and secondly by analyzing the amplitude noise of the reflection of the master laser from a Fabry-Pérot cavity. The line width of the clock transition was measured to be in the megahertz regime by spectroscopy and further characterized. The ac Stark shift of the ground level was investigated.

It was observed that the Doppler broadening must be highly reduced, or even eliminated, to achieve higher stability of the atomic clock. Finally the future perspectives and applications of optical lattices has been discussed.

Resumé

Forskningsfeltet inden for optiske atomure er af stor videnskabelig interesse, da stabiliteten og nøjagtigheden af atomure er markant højere i det optiske spektrum end i mikrobølge spektret. For at opnå høj nøjagtighed er det vigtigt at stabilisere frekvensen og karakterisere linjebredden af clock-laseren såvel som linjebredden af reference atomerne. I dette projekt blev clock-laseren og referenceatomerne i ^{24}Mg atomuret i laserlaboratoriet på Niels Bohr Institutet ved Københavns Universitet karakteriserede.

Linjebredden af master-laseren blev bestemt til at være i kilohertz området ved hjælp af to forskellige metoder. Først ved analyse af Pound-Drever-Hall errorsignalet og dernæst ved analyse af amplitudestøjen af master-laserens refleksion fra en Fabry-Pérot kavitét. Linjebredden af clock-overgangen blev karakteriseret og fundet til at være i megahertz området. Derudover blev ac Stark-skiftet af grundtilstanden undersøgt.

Det blev yderligere observeret, at Doppler bredden skal reduceres kraftigt, eller helst elimineres helt, for at opnå højere stabilitet. Slutteligt blev de fremtidige perspektiver af optiske fælder diskuteret.

Contents

1	Introduction	4
1.1	Challenges	5
1.2	This thesis	6
2	Characterization of the clock laser	6
2.1	Reference cavity line width	7
2.2	PDH error signal	11
2.3	Reflected amplitude noise signal	14
2.4	Clock laser	16
3	Characterization of the ^{24}Mg atoms in the MOT	17
3.1	Laser cooling	17
3.2	Spectroscopy of the $\text{Mg } ^3\text{P}_1 \leftrightarrow ^1\text{S}_0$ transition	18
3.3	Contributions to the atomic line width	21
3.3.1	Doppler width	21
3.4	ac Stark shift	22
4	Discussion	25
4.1	The future	27
5	Conclusion	28

1 Introduction

If you want to build a clock you basically need two elements: *an oscillator* with a well known frequency and *a counter* to count the oscillations. The first well known frequency standards were the oscillation of day and night, and the annual return of the seasons. These defined accurate time units to keep track of time. A frequency standard is a well known stable frequency from an oscillating system which can be used as a reference for a clock. As time units were developed by dividing the time in smaller intervals, such as the 24 hours of a day, higher frequency standards were needed.

In the 17th century mechanical pendulum clocks with great stability and accuracy were developed losing only one minute per day.

Later on in the 20th century the clock development accelerated. First by use of quartz crystals with a precision of losing only one second in three years, but even more importantly by the invention of the Caesium atomic clock which, in the beginning of the 21st century, had a loss of only one second in 30 million years! [1].

In atomic clocks the electric field of a laser is used as an oscillator. To ensure that the laser can be used as a frequency standard it is tuned into at a well defined frequency. Narrow banded atomic transitions are here used as references [1], such as the hyperfine transition in the Caesium clock or the forbidden singlet \leftrightarrow triplet transition in the magnesium optical clock. The former is with a number of atomic clocks in the JILA institute, Colorado USA, and in the SYRTE department of the Paris Observatory currently used in the SI definition of the second [2, 3]. The latter is investigated in the laser laboratory of the Niels Bohr Institute at the University of Copenhagen (NBI) as a possible optical clock transition similar to the optical Sr-atomic clocks in JILA and SYRTE [2, 3]. From now on we will refer to the laser used for the atomic clock at NBI as *the clock laser*.

A ^{24}Mg atom in Copenhagen is from quantum mechanics known to be identical with a ^{24}Mg atom in Paris or on Mars [4]. Hence by using well defined atomic transitions it is possible to have the exact same reference in experimental setups in different parts of the world, as long as the atoms are shielded from external perturbations such as electric and magnetic fields. This is one of the great advantages of the atomic clock, besides from being both more accurate and precise than any other type of clocks ever invented.

All clocks are characterized by their accuracy and stability. The accuracy of an atomic clock describes how well the frequency of the clock laser, ν_L , corresponds to the frequency of the atomic transition, ν_0 . The stability describes how much the measured clock frequency fluctuates over a given averaging time, τ [5]. The latter depends on the stability of the reference atoms and their lack of stability can be described by the Allan devia-

tion [5–7]:

$$\sigma(\tau) = \frac{\chi}{2\pi QS/N} \sqrt{\frac{t_c}{\tau}} \propto \frac{1}{Q} \sqrt{\frac{t_c}{N_a \tau}}. \quad (1)$$

$Q = \nu_{cl}/\delta\nu_{cl}$ is the quality factor of the clock transition with $\delta\nu_{cl}$ being the line width of the clock transition. S/N is the signal-to-noise ratio which in most cases is proportional with $\sqrt{N_a}$, where N_a is the number of reference atoms. Finally t_c is the measuring time and χ is a constant close to unity dependent on the probing method.

The Allan deviation is an analytically derived ideal statistical measure of frequency stability. Besides the quantities present in the expression for the Allan deviation, the stability of an atomic clock is determined by the frequency line width of the clock laser, $\delta\nu_L$, as a narrow transition line width requires a laser with a narrow line width to be measured. The stability is also determined by experimental conditions such as the floating of the clock laser frequency ν_L during the averaging time τ .

The development of atomic clocks in the microwave region has played a major role in various fields of science. The duration of one second has since 1967 been defined as 9 192 631 770 periods of the oscillating electric field from transition of the two hyperfine levels of the ground state of the Caesium-133 atom as mentioned above [2, 3]. The predictions of Einstein's theory of special relativity has been verified to a precision of 10^{-10} [1, pp. 244]. Furthermore the atomic clocks have made major improvement in navigation accuracy and the Global Positioning System (GPS) based on more than 24 satellites with atomic clocks is now applied everywhere in our everyday life.

1.1 Challenges

The attempt to obtain more stabilized atomic clocks gives us a number of challenges. Historically, the first atomic clocks were based on clock lasers in the microwave regime, $\nu \sim 10$ GHz. The reason being that the experimental setup did not allow measurements of oscillations faster than microwave frequencies [8]. In 2005 a Nobel prize was given for the development of an optical frequency comb [9], which made it possible to measure optical frequencies. The possibility for improvement of the atomic clock stability by using optical frequencies, $\nu \sim 5 \cdot 10^{14}$ Hz, is obvious when looking at the Allan deviation, Eq. (1), since $\sigma(\tau) \propto \nu_0^{-1}$ through the Q -factor and σ will be significantly decreased for greater clock transition frequencies. The stability can also be improved through the S/N -ratio by increasing N_a . This will increase the collisional shift of the the energy levels of the clock transition. Hence decrease both the accuracy and the stability of the atomic clock.

1.2 This thesis

In order to build an atomic clock we basically need a well defined and stabilized clock laser, a large amount of atoms, and a way to measure the oscillation of the clock frequency. Unfortunately the extend of this thesis do not us to go through all three subjects here, so we have chosen the first two.

The stabilization of the clock laser is of great importance for the stability of the clock and we will start in section 2 by investigating the laser system used at NBI. Here the clock laser is produced by frequency doubling a 914 nm laser, referred to as *the master laser*, which is stabilized by the Pound-Drever-Hall laser locking technique. The line width of this stabilized master laser is determined by two different methods in section 2.2 and 2.3 respectively.

The reference atomic system of laser cooled magnesium atoms trapped in a Magneto Optical Trap (MOT) is examined in section 3, and the line width of the clock transition is characterized. The Doppler broadening caused by the thermal movements of the magnesium atoms is of great importance, as the line width of the clock transition is strongly broadened by this. This broadening is determined in section 3.3.1. Magnesium atoms are laser cooled to reduce this broadening but since this cooling technique is based on the Doppler effect there is a lower limit for the temperature achieved [10].

A way of eliminating the Doppler broadening below the above mentioned limit, and one of the main topics in the atomic clock research field of today, is the use of an optical lattice. This uses a standing electromagnetic wave pattern inside a cavity system simulating a harmonic potential, in which the magnesium atoms can be trapped.

The reason for using atoms as frequency standards for atomic clocks were that the atomic systems are identical as long as the environments are well understood. However, if optical lattices are used for trapping atoms the atomic transition levels will be shifted by the ac Stark effect. If this shifted atomic transition is to be used as a reference for an atomic clock, the frequency of the clock transition needs to remain the same. Hence the energy levels need to be shifted equally. This ac Stark shift is investigated in section 3.4.

2 Characterization of the clock laser

In this chapter we are going to measure the line width of the 914 nm master laser which, after being frequency doubled to 457 nm, is used for the ^{24}Mg clock transition $^3\text{P}_1 \leftrightarrow ^1\text{S}_0$ ¹. We have used two different methods. The first one is based error signal obtained from the Pound-Drever-Hall (PDH) technique, while the second one uses photo detection of the reflected signal from the PDH reference cavity to analyze the noise amplitude of the signal, see Fig ???. Common for both methods is that we need to know the reference cavity line

¹Now and throughout the whole text $^3\text{P}_1$ and $^1\text{S}_0$ is used as abbreviations for $(3s3p)^3\text{P}_1$ and $(3s^2)^1\text{S}_0$ respectively.

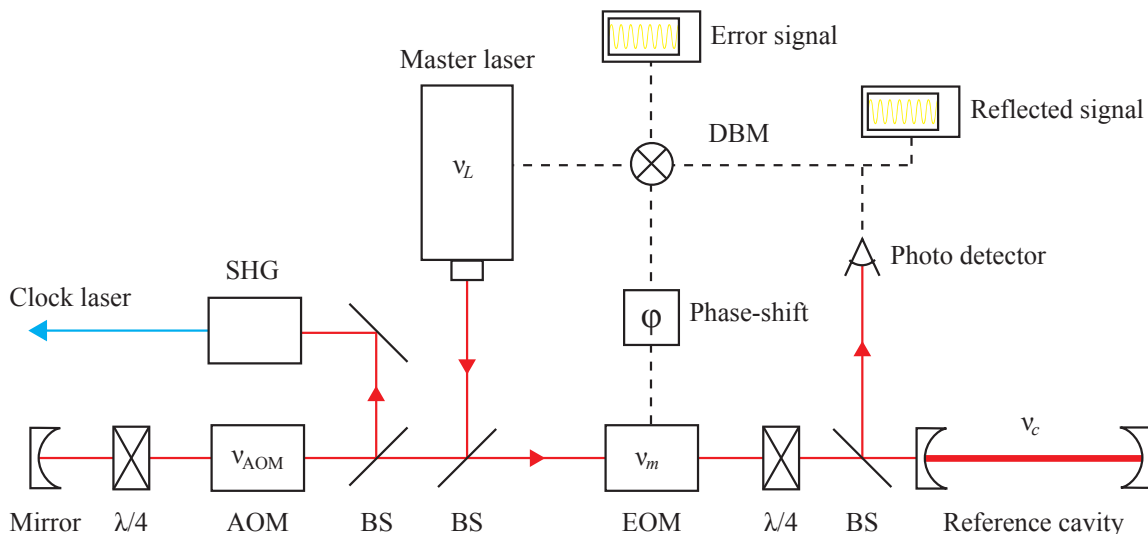


Figure 1: Sketch of the PDH setup. Solid lines are used for optical paths and dashed lines are used for signal paths. BS: Beam splitter, $\lambda/4$: λ -quarter plate, SHG: Second harmonic generator, DBM: Double Balance Mixer, AOM: Acousto-Optical Modulator, EOM: Electro Optical Modulator.

width to perform our data analysis. Therefore we start by going through measurements of the reference cavity ring-down from which we find its line width.

2.1 Reference cavity line width

To stabilize the frequency of the master laser we used the PDH technique, described in more details in the next section 2.2. This setup uses a very stable Fabry P rot cavity as a narrow band width reference by which the master laser can be locked to, see Fig. 1. The reference cavity has a line width due to the finite photon lifetime [11] and may be broadened by residual noise on the cavity such as vibrations and temperature fluctuations. As the cavity is used as a reference to the master laser its total line width contributes to the master lasers line width.

Stabilizing the cavity is done by placing it inside a vacuum chamber. The components of the cavity consists of, roughly speaking, two identical mirrors optically contacted onto a hollow glass rod (ultra low expansion (ULE) cavity). The ULE rests on another glass rod through two stabilizing Viton[®] O-rings [12], see Fig. 2.

To measure the reference cavity line width we used the technique of cavity ring-down. In a bare cavity, i.e., a cavity with no gain medium such as the reference cavity, the intensity decays exponentially as [11]:

$$I_c(t) = I_c(0) e^{-\delta\omega_c t}. \quad (2)$$

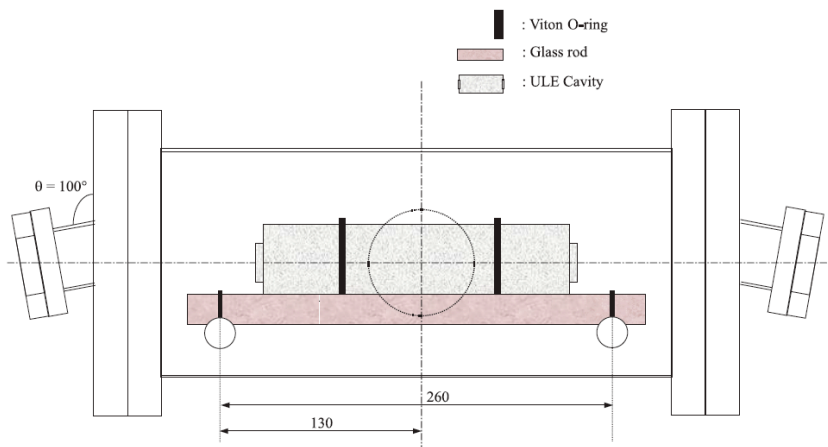


Figure 2: Sketch of the reference cavity. The beam of the master laser is send in along the horizontal axis through the ULE cavity. [12].

The finite photon lifetime inside the cavity is $\tau_c = 1/\delta\omega_c$ and depends on the cavity length L , its index of refraction n and its losses from transmission and scattering at the mirrors. By Fourier transforming the time-dependent cavity intensity the frequency spectrum is obtained and can be shown to have a Lorentzian lineshape

$$I_c(\nu) = I_c(0) \frac{1}{(2\pi)^{3/2}} \left(\frac{\delta\nu_c}{(\nu - \nu')^2 + \delta\nu_c^2} \right), \quad (3)$$

where the factor of $1/2\pi$ comes from the relation $\omega = 2\pi\nu$ and the factor of $1/\sqrt{2\pi}$ from the definition of the Fourier transform. The cavity line width is obtained from the Lorentzian function as the half width at half maximum (HWHM):

$$\text{HWHM} = \delta\nu_c = \frac{1}{2\pi\tau_c}. \quad (4)$$

Performing the measurements of the cavity ring-down we detected the reflected light from the reference cavity with a photodetector. This gave us a dc voltage signal on an oscilloscope with 10,000 data points each separated in time by 20 ns. At the day we performed our measurements we had problems triggering the signal. This prevented us from recording the cavity ring-down as scheduled. Instead we measured the build-up intensity inside the reference cavity, (Fig. 3). This does, however, not affect our results regarding the reference cavity line width since the characteristic time for the photon build-up process is equivalent to the decaying life time [13].

Starting with the master laser unlocked to the reference cavity, we tuned its frequency until the system was locked and then collected data with the oscilloscope. We made five measurements and fitted them to the intensity build-up equation:

$$I_c(t) = I_c(t_0)(1 - e^{-\delta\omega_c(t-t_0)}) + C, \quad (5)$$

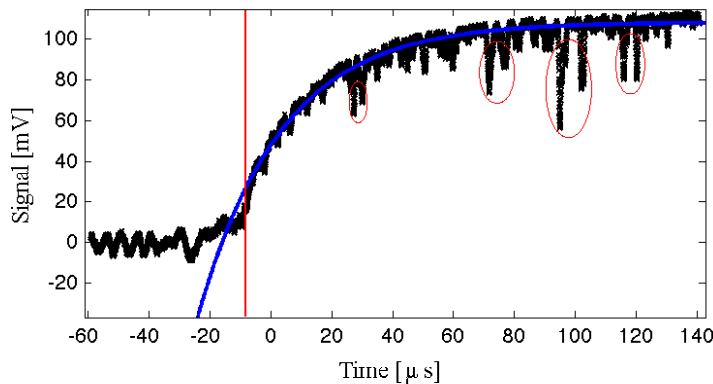


Figure 3: Example of data print of a build-up measurement. The black dots are data points, the blue line is the exponential fit, the red vertical line is the limit of the excluded points and the red circles mark points that were considered to be excluded due to their fluctuations.

by the method of robust nonlinear least squares with bisquare weights. Here $I_c(t_0)$ is the initial intensity, t_0 is the locking starting time (cf. $t_0 \approx -8 \mu\text{s}$ in Fig. 3), C is some constant and $\delta\omega_c$ is the angular frequency cavity (HWHM) line width satisfying the relations $\delta\omega_c = 1/\tau_c$ and $\delta\omega_c = 2\pi\delta\nu_c$, all are used as parameters in the fit.

Before fitting we excluded all data points lying before t_0 , such that it did not affect the fit (cf. the interval $t \in [-60 \mu\text{s}, -8 \mu\text{s}]$ in Fig. 3). We did not, however, exclude the seemingly large fluctuations encapsulated in circles in Fig. 3, since they do not change our obtained results.

We found that the fitted values depends strongly on where we choose to set the limit, t_0 before performing the fit. For example changing the limit by only $5 \mu\text{s}$ we found that the fitted value could be changed by up to $\sim 12 \%$. Performing several fits of each measurement, where we deviated the limit of excluded points by $5 \mu\text{s}$ in the interval $t \in [-25 \mu\text{s}, 0 \mu\text{s}]$, we obtained from each fit the reference cavity line width, $\delta\nu_c$. For every series of fits, concerning one build-up measurement, we estimated a value for $\delta\nu_c$ with minimal influence from the region before the build-up and with the largest number of data points still being contained in the fit.

To calculate the weighted average and uncertainty of the fitted values of the reference cavity line width, we have used the formulas [6]:

$$\delta\nu = \frac{1}{2\pi} \frac{\sum w_i \delta\omega_i}{\sum w_i} \quad \text{and} \quad \sigma_\nu = \frac{1}{2\pi} \frac{1}{\sqrt{\sum w_i}}, \quad (6)$$

where the weight w_i is being calculated from the uncertainties σ_i of the fitted value of

$\delta\omega_c$:

$$w_i = \frac{1}{\sigma_i^2}. \quad (7)$$

The factor of $1/2\pi$ in Eq. 6 comes from the fitted values to be given in units of rad/s whereas we are interested in having our results expressed in units of Hertz. From our five measurements we find the weighted average for the reference cavity (HWHM) line width to be:

$$\delta\nu_c = 5.61 \pm 0.02 \text{ kHz}. \quad (8)$$

The fitted values and their fit uncertainties as error-bars has been plotted together with $\delta\nu_c$ in Fig. 4.

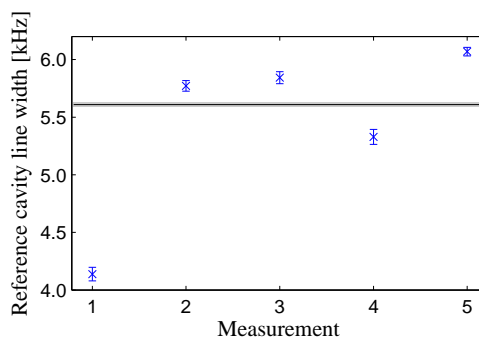


Figure 4: Plot of the fitted values and fit uncertainties of the reference cavity (HWHM) line width as blue crosses with error-bars. The black horizontal line shows the weighted average with the weighted uncertainty as the grey area, $\delta\nu_c$.

Measurement 1 deviates almost 30 % from $\delta\nu_c$, whereas the other four measurements deviates by less than 8 %. Comparing the build-up plot of measurement 1 with the other plots it was seen to fluctuate more. This, together with its large deviation, made us discard it from our further analysis. From Fig. 4 it is also seen that none of the results coincides with $\delta\nu_c$, suggesting that their individual uncertainties are too small. This is most likely due to the MATLAB fitting method underestimating the uncertainties by using $N \sim 10\,000$ data points to calculate the uncertainty as $\propto 1/\sqrt{N}$.

To obtain a more reasonable value of the reference cavity line width we calculate instead the mean value and standard deviation (SD) of mean by [6]:

$$\delta\nu = \frac{1}{2\pi N} \sum_{i=1}^N \delta\omega_i \quad \text{and} \quad \sigma_\nu = \frac{\text{SD}}{\sqrt{N}} = \frac{1}{\sqrt{N}} \sqrt{\frac{1}{N-1} \sum_{i=1}^N \left(\frac{\delta\omega_i}{2\pi} - \delta\nu \right)^2}. \quad (9)$$

From this we now obtain the reference cavity (HWHM) line width to be:

$$\delta\nu_c = 5.8 \pm 0.2 \text{ kHz}. \quad (10)$$

This value for the reference cavity line width is the one used for further analysis in the next sections. A plot of the fitted values with the SD as error-bars together with $\delta\nu_c$ is shown in Fig. 5. All four values are seen to coincide with $\delta\nu_c$.

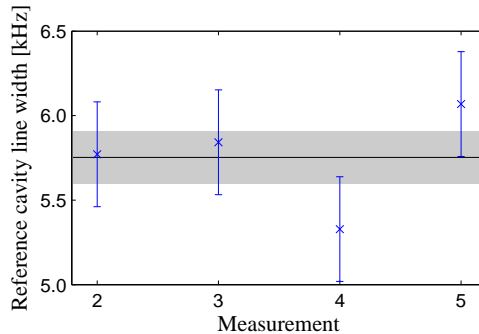


Figure 5: Plot of the fitted values and SD uncertainties of the reference cavity (HWHM) line width as blue crosses with error-bars. The black horizontal line shows the mean value with the SD of mean as the grey area, $\delta\nu_c$.

2.2 PDH error signal

The (HWHM) line width of the reference cavity is now established to be $\delta\nu_c = 5.8 \pm 0.2$ kHz and we can proceed to find the line width of the master laser by using the Pound-Drever-Hall laser stabilization technique [1, 14].

In the Pound-Drever-Hall setup we apply two sidebands, with frequencies $\nu_L \pm \nu_m$, to the master laser, with frequency ν_L , by using an Electro Optical Modulator (EOM), cf. Fig 1. These sidebands are applied by modulating the phase of our electric field periodically with a frequency $\nu_m = 1$ MHz.

The master laser with the two sidebands are sent into the reference cavity and a photodetector measures the reflected light consisting of all the reflections from both the first and second mirror in the reference cavity. At resonance frequency the phase shift of the electromagnetic field from one round trip in the reference cavity is π . The sum of all round trip components inside the cavity is now making standing waves, while the reflected beam outside the cavity is canceled out by destructive interference [14].

The signal detected by the photodetector is sent into a double balance mixer (DBM) and mixed together with a signal from the EOM with the frequency ν_m . The outgoing error signal, $V(\Delta\nu)$, is the product of the two signals and is proportional to [1]:

$$V(\Delta\nu) \propto -4 \frac{\nu_m^2 (\Gamma/2) \Delta\nu [(\Gamma/2)^2 - \Delta\nu^2 + \nu_m^2]}{[(\Gamma/2)^2 + \Delta\nu^2][(\Delta\nu - \nu_m)^2 + (\Gamma/2)^2][(\Delta\nu + \nu_m)^2 + (\Gamma/2)^2]}, \quad (11)$$

where $\Gamma = 2\pi\delta\nu_c$ and $\Delta\nu = \nu_L - \nu_c$ is the detuning of the frequency of the master laser, ν_L ,

and the cavity resonance frequency, ν_c . This unitless coefficient is called the D -coefficient throughout the text and it has maximum/minimum values of $D_{max/min} = \pm 2$.

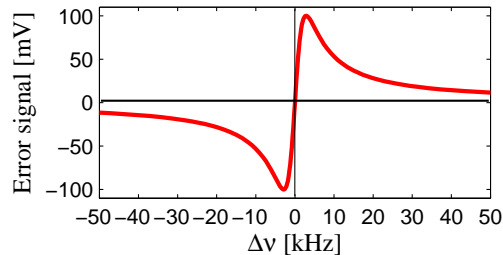


Figure 6: Plot of $V(\Delta\nu) = C_p D(\Delta\nu)$.

The experimental setup did not allow us to scan the error signal for different values of $\Delta\nu$ and thus measure the $V(\Delta\nu)$ profile. However, the maximum and minimum value of the error signal can be estimated by detecting the peaks of the error signal. From this we found $V_{max/min} \sim \pm 100$ mV. Knowing these values and the shape of $V(\Delta\nu)$ we can multiply the D -coefficient with a proportionality constant $C_p = V_{max}/D_{max} = 100 \text{ mV}/2 = 50 \text{ mV}$, and obtain the calculated signal as $V(\Delta\nu) = C_p D(\Delta\nu)$ (Fig. 6). This allows us to make further calculations of the frequency line width of the master laser.

A measurement of the error signal over time reveals a Gaussian distribution of the ac signal from the photodetector. This corresponds to Gaussian distributed fluctuations in the reflected intensity from the reference cavity which corresponds to fluctuations of the detuning $\Delta\nu$. To find the full width half maximum (FWHM) of the frequency of the error-signal we can project the error signal onto the profile of $V(\Delta\nu)$, see Fig. 7.

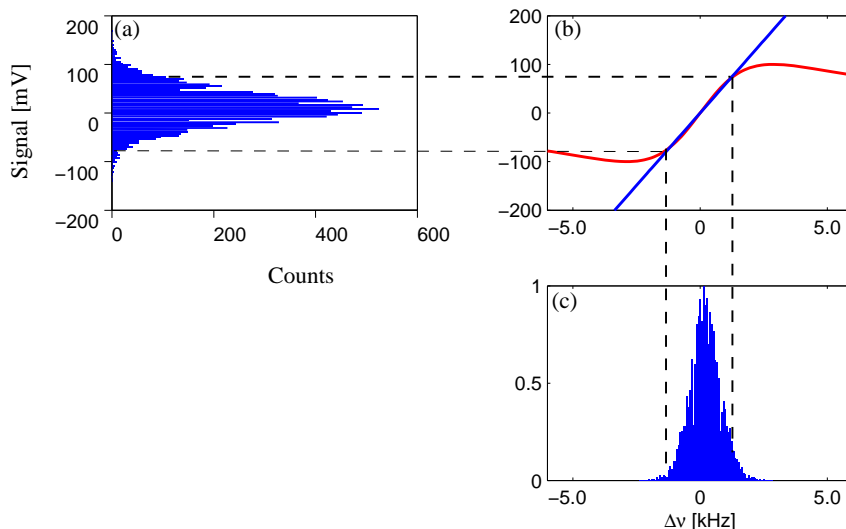


Figure 7: (a) Signal distribution of measurement 2 projected onto the linear approximation (blue line) of the error-signal (red curve) (b). Each projected point gives a point on the frequency axis for the master lasers intensity distribution (c).

For simplicity we assumed that $V(\Delta\nu)$ is linear in the interval $\Delta\nu \approx 0$ and approximated it with the linear function $V = (70 \text{ mV}/1013 \text{ Hz})\Delta\nu$, see Fig. 7(b). This approximation has some limitations. Outside the interval $[-70 \text{ mV}, 70 \text{ mV}]$ the difference of the frequency value from a projection onto the linear approximation and onto the $V(\Delta\nu)$ profile reveals a difference up to $\sim 50\%$. A minor fraction of our data points of the error signal is even outside the interval $[-100 \text{ mV}, 100 \text{ mV}]$. Hence it is not possible to project signals outside this interval onto the $V(\Delta\nu)$ profile. However, 95% of the error signal lie inside the interval $[-70 \text{ mV}, 70 \text{ mV}]$. Data points outside this interval will thus not give any significant contribution to the line width and can be neglected.

We performed six measurements of the error signal and found the mean value of the master laser (FWHM) line width and the SD of mean, using Eq. (9), to:

$$\delta\nu_L = 1.2 \pm 0.2 \text{ kHz}. \quad (12)$$

The relative uncertainty of $\sigma_\nu/\delta\nu_L \approx 0.2$ is an acceptable result considering the linearly approximation of the predicted error signal profile and the very imprecise measurement of V_{max} for which we found a variation of 10 % resulted in a corresponding variation of the FWHM of $\approx 10 \%$.

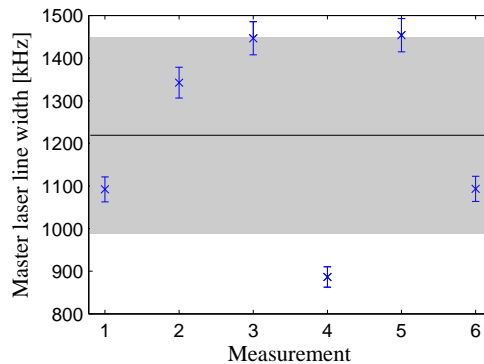


Figure 8: Plot of the fitted values of the master laser (FWHM) line width and their uncertainties rising from the uncertainty of the reference cavity line width. The black horizontal line shows the mean value with the SD of mean as the grey area.

$\delta\nu_L$ is together with the six fits of the error signals plotted in Fig. 8. The error-bars represent the propagated uncertainties from the PDH reference cavity line width used in Eq. (11) for $V(\Delta\nu)$.

2.3 Reflected amplitude noise signal

A second way by which we determined the master laser line width, is by analyzing the amplitude noise of the reflected light from the reference cavity in the PDH setup (cf. the previous section 2.2). The reflected light from the cavity can be detected by a high bandwidth photodetector and used to generate a dc signal on an oscilloscope fluctuating with the laser frequency [14]. Note that contrary to the PDH error signal, this signal is not mixed with the modulation signal, but is the pure reflected signal from the reference cavity.

The beam hitting the reference cavity consist of both the master laser frequency, ν_L , and its sidebands frequencies from the EOM, $\nu_L \pm \nu_m$. When the master laser is locked to the reference cavity the reflected light, arising from all the roundtrip contributions of the master laser, interfere destructively with itself. Hence the locked reflected signal consist only of the sideband reflections [14]. When the master laser is unlocked to the reference cavity the reflected signal will therefore be greater opposed to when it is locked.

For each measurement we noted the mean values of both the locked and unlocked signal for further use in our data analysis, since these quantities can be used to set a scale of the intensity, I , letting the locked signal $V_{\text{locked}} \rightarrow I/I_{\text{max}} = 1$ and $V_{\text{unlocked}} \rightarrow I = 0$. In practice we have used the conversion factor:

$$I/I_{\text{max}} = \frac{V - V_{\text{unlocked}}}{V_{\text{locked}} - V_{\text{unlocked}}}, \quad (13)$$

where V is the data point of our signal of which we would want to know the corresponding intensity. We use I/I_{\max} instead of just I such that the intensity is scaled to be a dimensionless quantity between 0 and 1. This is sufficient since we are only interested in the line width and not the intensity as such.

We expect the intensity distribution of the master laser as a function of frequency to be a Gaussian distribution with maximum value, $I/I_{\max} = 1$, at the frequency ν_L . Any frequency fluctuation, δ , from ν_L , i.e., any amplitude noise in the detected signal, is thus expected to be seen as a greater signal than the signal for ν_L , regardless of the sign of δ . The profile is thus expected to have a shape as in Fig. 9(a) with a cut-off at the signal value corresponding to I_{\max} . Note that a greater signal corresponds to a greater *negative* signal on the oscilloscope.

When plotting our measured signal distribution and fitting them we found a Lorentzian distribution on the left side of the mean value, i.e., V_{locked} , and a Gaussian distribution on the right side, cf. Fig. 9(b).

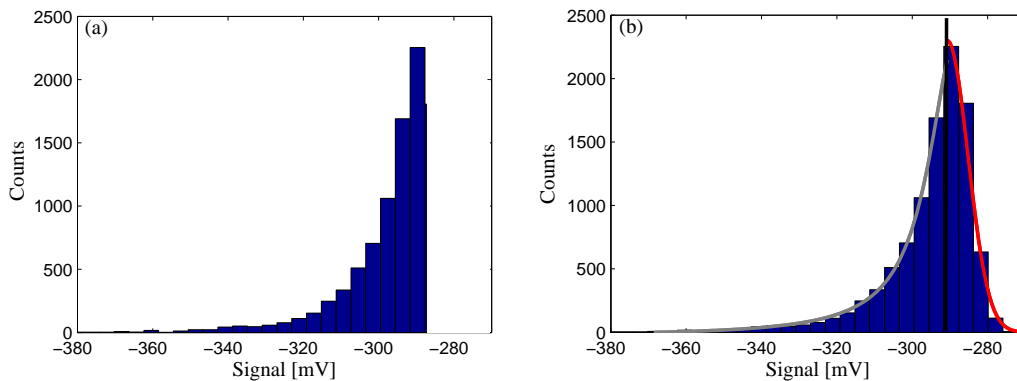


Figure 9: (a) *Histogram showing the expected distribution of the reflected signal.* (b) *28 bin histogram over the signal fluctuations. The grey curve is a Lorentzian fit, and is seen to match the histogram to the left of the mean value marked with a black vertical line. The red curve is a Gaussian fit and is seen to fit the right side of the histogram.*

Since the signal to the right of V_{locked} is not expected, we can immediately recognize this Gaussian distribution as frequency noise coming from the electronic or other devices in our setup and *not* as noise from the master lasers frequency. The electronic noise is a symmetric convolution through the whole signal [1]. For further analysis we have approximated the Gaussian noise to be a delta Dirac function, thus neglecting it.

With the conversion factor in hand, Eq. (13), we can for each bin in the histogram find the corresponding deviation in the frequency from ν_L , by projecting it onto the Lorentzian plot of the reference cavity intensity distribution found in section 2.1, see Fig. 10.

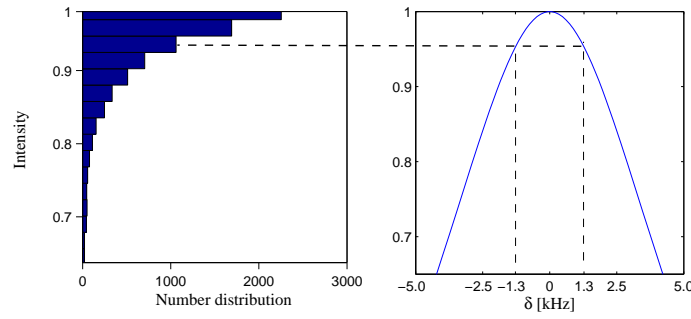


Figure 10: *Signal distribution of measurement 1 (left) projected onto the reference cavity intensity distribution (right). Each data point gives two points on the frequency axis for the master lasers intensity distribution. On the right figure the (FWHM) line width of the master laser has been marked as ranging from $\delta = -1.3$ kHz to $\delta = 1.3$ kHz.*

For each histogram projected onto the reference cavity intensity distribution, we fitted the obtained master laser intensity distributions with a Gaussian function, Eq. (17), and found the master laser (FWHM) line width, using Eq. (9), to be:

$$\delta\nu_L = 2.2 \pm 0.1 \text{ kHz} . \quad (14)$$

The fitted values with their individual uncertainties, rising from the uncertainty of the reference cavity line width, as error-bars has been plotted together with $\delta\nu_L$ in Fig. 11.

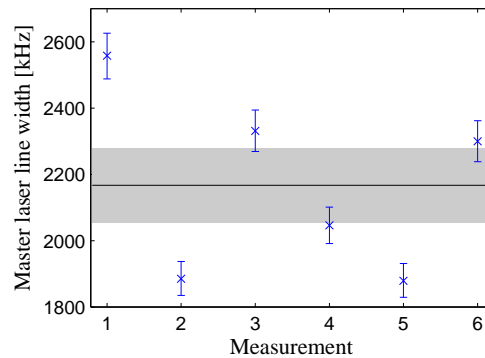


Figure 11: *Plot of the fitted values of the master laser (FWHM) line width and their uncertainties rising from the uncertainty of the reference cavity line width. The black horizontal line shows the mean value with the SD of mean as the grey area.*

2.4 Clock laser

With the 914 nm master laser now stabilized in the kilohertz regime, it can sent into an external ring cavity and frequency doubled by second harmonic generation (SHG) to a wavelength of 457 nm. This is done using a non linear potassium niobate crystal

(KNbO_3) [15] (cf. Fig. 1). Hereby the FWHM line width of the clock laser is estimated to be twice the line width of the master laser:

$$\delta\nu_L \pm \sigma_\nu \rightarrow \delta\nu_{457} = 2\delta\nu_L \pm 2\sigma_\nu \quad (15)$$

A blue 457 nm laser can also be achieved using infrared Ti:Sapphire lasers. However, the frequency control of a Ti:Sapphire laser is done mechanically by use of geometric or piezoelectric elements and this sets an upper limit for the frequency control bandwidth in the 10 kHz region. The frequency control of a diode laser is much faster as it is based on current control. This frequency control bandwidth is approximately 10 MHz and the feedback time is thus much less than what can be achieved by the Ti:Sapphire laser. Because of this the diode laser is preferred.

3 Characterization of the ^{24}Mg atoms in the MOT

With the characterization of the clock laser we can now examine the properties of the magnesium atoms used as reference for the atomic clock. The following chapter is concerning two different measurements. As the stability of an atomic clock depends on the absorption line width of the clock transition it is of great interest to measure this. However, many broadenings are contributing to this line width and the Doppler broadening from the thermal fluctuations will here be of special interest. This will be discussed in section 3.3.

Another subject of great importance for the accuracy and stability of the atomic clock is the environment of the reference atoms to be well defined. If an uncharacterized external perturbation is applied to the clock transition, and this shifts the transition frequency, then the clock frequency and thereby the accuracy of the clock will be changed. An external perturbation to be mentioned is the ac Stark shift. The extent and importance of this effect is discussed in section 3.4 and 4.

3.1 Laser cooling

Consider a neutral magnesium atom as a two level atom with a transition frequency ν_0 placed at rest in an electromagnetic field. If the frequency of the electromagnetic field, ν , is tuned below the transition frequency ν_0 nothing will happen.

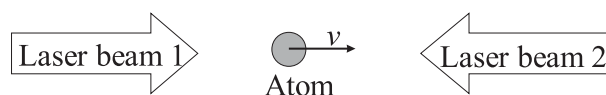


Figure 12: *Laser cooling in one dimension using the Doppler effect [12].*

If the atom is now traveling with a velocity, \vec{v} , in the opposite direction of the propagation of the electromagnetic field, as in Fig. 12 for the atom and laser beam 2, then it will experience the Doppler shifted frequency [11]:

$$\nu' = \nu \left(1 + \frac{v}{c} \right), \quad (16)$$

where c is the speed of light $v \ll c$. If $\nu \approx \nu_0$ then, for a given velocity, the frequency ν' will be shifted up to ν_0 . The atom will now absorb a photon from laser beam 2 and thus receives a momentum, $\hbar\vec{k}$, pointing in the opposite direction of \vec{v} . Hence slowing the atom down due to conservation of momentum. The re-emission of the photon by spontaneous emission occurs in an arbitrary direction. If the laser intensity is much less than the saturation intensity of the transition, the spontaneous emission will dominate compared to stimulated emission (see Eq. (19) for the expression of the saturation intensity). The spontaneous emitted photons from a cloud of atoms transfer more energy out of the system than the system receives from the trapping laser. This gives a negative shift of the velocity distribution of the atoms and the temperature will fall according to the Maxwell-Boltzmann distribution [11].

If the process is continued an atom will eventually have its velocity reversed and therefore another laser beam is needed working in the opposite direction. This is laser beam 1 in Fig. 12. At NBI six laser beams are used for cooling a cloud of ^{24}Mg atoms which have first been trapped by the MOT. For the clock transition $^3P_1 \leftrightarrow ^1S_0$ in ^{24}Mg , investigated in this thesis, the two levels 1P_1 and 1S_0 are used for laser cooling by a 285 nm trapping laser.

3.2 Spectroscopy of the Mg $^3P_1 \leftrightarrow ^1S_0$ transition

With our characterization of our laser system we are now ready to investigate the properties of the clock transitions of magnesium for the atomic clock. We will extend our work with the magnesium by characterizing the different broadenings.

The transitions of interest in our work are the $^3P_1 \leftrightarrow ^1S_0$ (transition) and the $^1P_1 \leftrightarrow ^1S_0$ (transition), see Fig. 13. The latter transition is a broadband singlet \leftrightarrow singlet transition (~ 80 MHz) [15] used for laser cooling. The first transition, on the contrary, is a singlet \leftrightarrow triplet transition which is forbidden to all orders by the LS -coupling selection rules for $\Delta S = 0$ [10]. Thus, the natural bandwidth of this transition is very narrow (~ 30 Hz) [12]. The $^3P_1 \leftrightarrow ^1S_0$ transition wavelength is 457 nm.

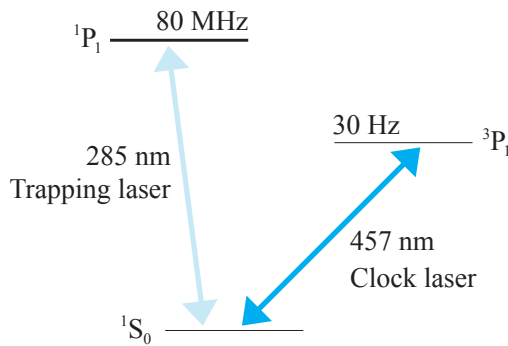


Figure 13: The $^3P_1 \leftrightarrow ^1S_0$ transition and the $^1P_1 \leftrightarrow ^1S_0$ transition

This makes the $^3P_1 \leftrightarrow ^1S_0$ transition an ideal clock transition as a small clock transition line width improves the precision of the atomic clock, cf. Allan deviation from Eq. (1). As we send our PDH stabilized 457 nm laser into the MOT we will eventually excite some of the atoms to the 3P_1 state.

The intensity of the fluorescence due to the spontaneous emission from the $^1P_1 \leftrightarrow ^1S_0$ transition for laser cooling is dependent of the number of ^{24}Mg atoms in the ground state 1S_0 . Since we measure the intensity of the fluorescence a loss of the number of atoms in the ground state induced by scanning over the $^3P_1 \leftrightarrow ^1S_0$ transition can be directly seen as a reduction in the fluorescence intensity. So by measuring the intensity of the $^1P_1 \leftrightarrow ^1S_0$ fluorescence, we can measure the line width of the $^3P_1 \leftrightarrow ^1S_0$ transition.

The scan of the $^1P_1 \leftrightarrow ^1S_0$ fluorescence was performed using an Acousto-Optical Modulator (AOM). The AOM modulates the 914 nm laser twice by a frequency ν_{AOM} before it is frequency doubled by being sent through a non-linear crystal generating second harmonics [11]

The total modulation of the 457 nm laser is thus $4\nu_{\text{AOM}}$, cf. Fig. 1. By modulating the frequency we vary the loss of the number of the 1S_0 state induced by the clock laser and we measured a drop in the intensity in the modulation range 270-290 MHz. Our measurements revealed in each case a double peak. Making Gaussian fits,

$$G(\nu) = \frac{1}{\sigma\sqrt{2\pi}} e^{-\frac{(\nu-\nu_0)^2}{2\sigma^2}}, \quad (17)$$

for each of the two peaks we obtain the two different full width at half maximum $\text{FWHM} = 2\sigma\sqrt{2\ln 2}$. When fitting the peaks separately with Gaussian fits we excluded data points from the other peak just as we excluded obvious experimental errors caused by disturbing elements and sudden noise present in the experimental environment at the experiment sessions, see Fig. 14.

In many experiment series we excluded a number of the first data points as they were fluctuating from the steady level of the fluorescent of our magnesium cloud.

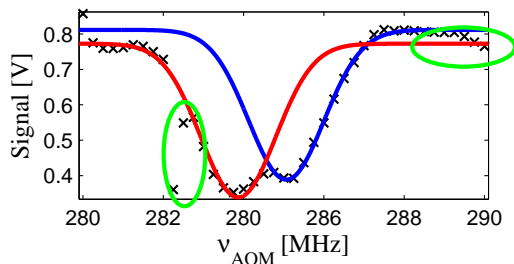


Figure 14: Gaussian fits for each peak. In green: Excluded data points.

This splitting of the peaks was not expected. This could be caused by a Doppler shift of the transition frequency and the two separate peaks indicate that there are two different velocity components for the magnesium atoms in the MOT. The difference of the two peaks $\delta\nu_{peaks}$ is $\delta\nu_{peaks} \approx 4$ MHz. From the Doppler theory, $\Delta\nu/\nu = v/c$, this difference corresponds to a speed difference in the MOT of $\Delta v \approx 1.8$ m s $^{-1}$. Rotational movements of the magnesium cloud in the MOT did not cause the two separate velocities as the 457 nm clock laser was sent into the magnesium cloud from only one direction and the velocity distribution of a rotational cloud should be continuous. If the clock laser was sent in from two different directions, different velocity components could occur. However, the clock laser was aligned such that possible reflections of the clock laser was aligned away from the magnesium cloud. Another possibility is that the clock laser was locked on the TEM $_{1,0}$ -mode instead of the TEM $_{0,0}$. At the experimental setup the fluorescent was constantly monitored by a CCD camera and it is very unlikely that the clock laser was locked on the TEM $_{1,0}$ -mode. However, a TEM $_{1,0}$ will correspond to two parallel beams and they will excite atoms in different parts of the magnesium cloud. If the cloud is rotating the two parts of a TEM $_{1,0}$ -mode will experience different velocity components. We have calculated the weighted average and the weighted uncertainty of the clock transition (FWHM) line width by using Eq. (6) and have listed the results for each peak in Table 1.

Peak	$\delta\nu_{cl}$ [MHz]
Left	11.24 ± 0.28
Right	12.28 ± 0.32

Table 1: The FWHM of the two peaks of the absorption spectrum of the clock transition.

This choice of Gaussian fits will be discussed later in this section. The above results are calculated from the measurements with the 285 nm trapping laser turned off when the clock laser was tuned on as required for a scan measurement. The measurements with

both the trapping laser and the clock laser turned on simultaneously for measuring the ac Stark shift is discussed in section 3.4.

3.3 Contributions to the atomic line width

The width of the peaks must consist of contributions from different kinds of broadenings where the most significant are Doppler broadening $\delta\nu_D$, power broadening $\delta\nu_p$, the laser line width of the 457 nm clock laser $\delta\nu_{457}$ and the natural line width of the 3P_1 state $\delta\nu_0$. Assuming that all the contributions are independent of each other, we expect that the final line width can be written on the form [6]:

$$\delta\nu_{cl} = \sqrt{\delta\nu_0^2 + \delta\nu_{457}^2 + \delta\nu_p^2 + \delta\nu_D^2}. \quad (18)$$

The natural line width is $\delta\nu_0 \sim 30$ Hz [12], the clock laser line width was measured in section 2.2 to $\delta\nu_{457} = 2 \cdot 1.2$ kHz = 2.4 kHz and the power broadening can be calculated as [10]:

$$\delta\nu_p = \delta\nu_0 \sqrt{1 + \frac{I}{I_{sat}}} = 59.0 \text{ kHz} \quad \text{for} \quad I_{sat} = \frac{\pi}{3} \frac{hc}{\tau\lambda^3}. \quad (19)$$

We found the measured width of absorption profile to be in the MHz regime. From the three expected contributions to the line width of the $^3P_1 \leftrightarrow ^1S_0$ transition plus our measured value of the line width, we are now, from Eq. (18), able to predict that the Doppler width should be in the MHz regime, since

$$\delta\nu_D = \sqrt{\underbrace{\delta\nu_{cl}^2}_{MHz} - \underbrace{\delta\nu_0^2}_{Hz} - \underbrace{\delta\nu_{457}^2}_{kHz} - \underbrace{\delta\nu_p^2}_{kHz}} = \begin{cases} 11.24 \text{ MHz} & \text{for left peak} \\ 12.28 \text{ MHz} & \text{for right peak} \end{cases} \quad (20)$$

It is seen that the Doppler broadening is dominating and $\delta\nu_D \approx \delta\nu_{cl}$. The Doppler profile is a Gaussian distribution [11], so the use of Gaussian fits is consistent with our theory.

3.3.1 Doppler width

The contribution to the FWHM from the Doppler broadening can be calculated from the Maxwell-Boltzmann distribution [11, pp. 103]:

$$\delta\nu_D = 2 \frac{\nu_0}{c} \sqrt{\frac{2k_B T}{m} \ln 2}, \quad (21)$$

where ν_0 is the transition frequency between the 1P_1 and 1S_0 states, c is the speed of light, k_B is the Boltzmann constant and T and m are the temperature and the mass of the magnesium atoms respectively.

From our results in Table 1 we can calculate a temperature for the MOT:

Peak	T [mK]
Left	14.0
Right	16.6

Table 2: *Temperatures corresponding to the two transition (FWHM) line widths of the absorption spectrum, cf. Table 1.*

The temperature of the MOT in the setup is in previous experiments measured to be approximately $T \sim 5$ mK [15]. The temperatures calculated from the two measured FWHM are both above this value, and a Doppler width corresponding to the temperature of 5 mK should be $\delta\nu_D \sim 6.76$ MHz. However, this high temperature can be caused by too high detuning of the 285 nm trapping laser or alignment problems for the six trapping lasers. Since the intensity profile of the trapping laser is not purely Gaussian, alignment problems can have caused asymmetric distribution of the ^{24}Mg atoms and rotational movements in the MOT. This could explain both the high temperature and the double peak structure. In any case the Doppler broadening is in the megahertz regime and this supports the assumption that the Doppler width is the dominant contribution to the absorption line width of the contributions presented in Eq. (18).

We have mentioned that an ideal clock transition has a small natural line width in the hertz region. However, we have in the previous section shown that the Doppler width in the temperature of our experimental setup is in the megahertz region and the natural line width of the clock transition will be negligible in the presence of Doppler broadening. Further cooling by laser cooling is not an option since the lower limit for temperature achieved by laser cooling is the Doppler temperature [10]:

$$T_D = \frac{\hbar\Gamma}{2k_B} \approx 2 \text{ mK}. \quad (22)$$

This corresponds to a Doppler width of ≈ 4 MHz. A method for eliminating the Doppler broadening is, by use of optical lattices, based on the ac Stark shift of the transition frequencies. The ac Stark shift will be examined in the following section 3.4 and the future perspectives of the optical lattice will be discussed in chapter 4.

3.4 ac Stark shift

In the preceding development of the atomic clock, it has been found that trapping the atoms in a standing wave light pattern, i.e., an optical lattice, can improve both the accuracy and stability of the atomic clock [16,17]. When the atoms are being restricted to this simulated harmonic potential they are confined in the Lamb-Dicke regime, meaning that they are localized within a range smaller than an optical wavelength [18]. Hence

eliminating the broadening and frequency shift of the atoms by, e.g., the Doppler effect and recoil motion.

Aside from acting as a dipole trap for the atoms, the electric field of the standing wave also perturbs the energy levels of the clock states, thus inducing a light shift (actually the light shift *is* the dipole potential) [10]. This is the *ac Stark shift* and the shifted frequency of the clock transition is given by the difference in the perturbed energy levels as [19]:

$$\delta\nu_{\text{Stark}}(\omega_L) = \frac{1}{h}[\delta E_e(\mathbf{E}, \omega_L) - \delta E_g(\mathbf{E}, \omega_L)], \quad (23)$$

with δE_i being the frequency shift of level i , the indices e and g representing the upper and lower level of the clock transition respectively, i.e. 3P_1 and 1S_0 , and ω_L and \mathbf{E} being the angular frequency and polarization of the trapping laser.

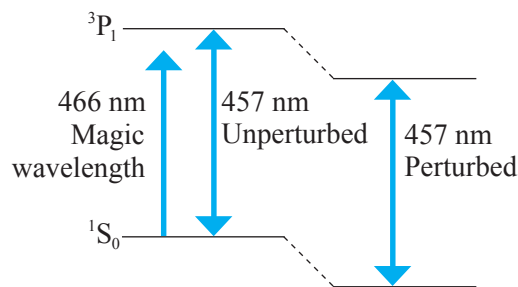


Figure 15: Energy diagram showing the *ac Stark shift* of the ^{24}Mg clock levels 1S_0 and 3P_1 when perturbed by the magic wavelength.

If the trapping laser is such that \mathbf{E} and ω_L satisfy $\delta\nu_{\text{Stark}} = 0$, then the optical lattice can be very advantageous as an atomic clock and may set new frequency standards with a stability of $\sim 10^{-15}$ [7, 20]. This condition is called the *magic wavelength*, see Fig. 15.

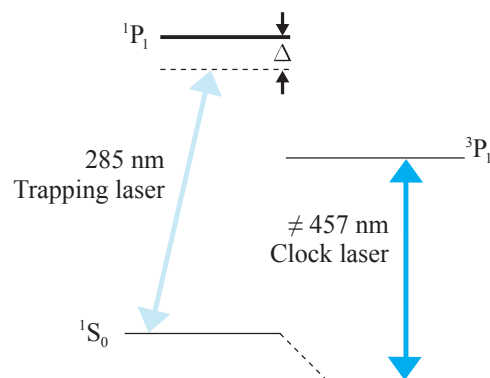


Figure 16: Energy diagram showing the *ac Stark shift* of the 1S_0 ground state. The frequency of the perturbed clock transition is greater than for the unperturbed case. Δ is the detuning of the 285 nm trapping laser from the 1P_1 level.

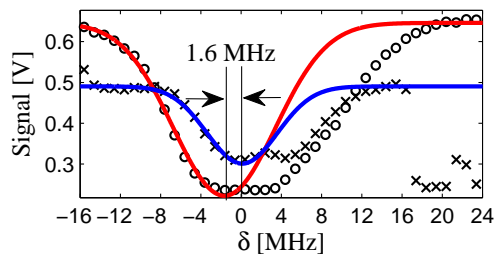


Figure 17: Absorption spectra of two measurements of the $Mg\ ^3P_1 \leftrightarrow\ ^1S_0$ clock transition for (i) regular spectroscopy (black crosses) and (ii) ac Stark induced spectroscopy (black circles). Both spectra (i) and (ii) has been fitted by the Gaussian blue and red curves respectively. The detuning δ is set to zero at the peak of the regular clock spectrum.

Measuring the ac Stark shift we used the same setup as for measuring the line width of the $Mg\ ^3P_1 \leftrightarrow\ ^1S_0$ clock transition, but without turning off the 285 nm trapping laser while scanning. This should induce the ac Stark shift, and we expect to find the same absorption profile as before. Calculating the ac Stark shift of the clock states yields a much greater shift of the lower state than the upper state, such that the shift of the upper level can be neglected, cf. Fig. 16. The clock transition frequency will now be shifted since the, now perturbed, ground state eigenenergy will be shifted. This is seen as a shifted peak value of the absorption spectrum in Fig. 17. Note that we measure the ac Stark shift of the ground state, $\Delta\nu_{\text{Stark}}$, and not of the clock transitions frequency, $\delta\nu_{\text{Stark}}$. The red-tuned trapping laser gives a negative ac Stark shift of the ground state energy [18].

Performing 3 measurements and using the same fitting and calculation method as in section 3.2, we have calculated the peak value of the clock transitions frequency. Taking the difference of the peak value of the unperturbed measurements we obtain an ac Stark shift of the ground state given as $\Delta\nu_{\text{Stark}} = 1.96 \pm 0.27$ MHz.

The plot in Fig. 17 also reveals a change of the clock transitions line width having a greater value. This effect could be caused by amplitude and frequency noise from the 285 nm trapping laser now being on during the whole measurement.

To validate the experimental values of the ac Stark shift of the clock transition we have calculated the light shift of the 1S_0 ground state using the expression [18]:

$$\Delta\omega_{\text{Stark}} = \frac{1}{2} [\Omega_n(\Delta) - \Delta], \quad (24)$$

here $\hbar\Omega_n(\Delta)$ and $\hbar\Delta$ are the energy difference between the perturbed and unperturbed states respectively. $\Delta = \omega_0 - \omega$ is the detuning of the $^{24}\text{Mg}\ ^1P_1 \leftrightarrow\ ^1S_0$ cooling transition with ω_0 being the frequency difference between the two levels and ω the 285 nm trapping

laser frequency. $\Omega_n(\Delta)$ is the Rabi frequency given by [18]:

$$\Omega_n(\Delta) = [\Omega_n^2(\Delta = 0) + \Delta^2]^{1/2}. \quad (25)$$

$\Omega_n(\Delta = 0)$ depends on the number of photons in the field and the coupling strength between field and atoms. Both of these quantities are difficult to work with, so instead of using the quantum mechanical description of the Rabi frequency we approximate it by its analogous classical quantity, Ω , which can be expressed [10]:

$$\Omega = \Gamma \left(\frac{I}{2I_{\text{sat}}} \right)^{1/2}, \quad (26)$$

where Γ is the line width of the $^1P_1 \leftrightarrow ^1S_0$ transition and I and I_{sat} are the intensity and saturated intensity of the 285 nm trapping laser respectively (cf. Eq. 19 for the expression of I_{sat}). The above approximation is allowed as long as the light field contains $n \gg 1$ photons. Furthermore, laser light is a coherent state, i.e., the most classical state of light also supporting the approximation [18]. The ac Stark shift can now be given as:

$$\Delta\nu_{\text{Stark}} = \frac{1}{2} \left[\left(\Gamma^2 \left(\frac{I}{2I_{\text{sat}}} \right) + \Delta^2 \right)^{1/2} - \Delta \right]. \quad (27)$$

Before the trapping laser is sent into the vacuum chamber where the MOT is localized, its beam is split into three equal sized beams, which are then sent into the vacuum chamber from three orthogonal directions. After passing through, all three beams are reflected back into the vacuum chamber such that the magnesium atoms are laser cooled as described in section 3.1. Measuring the power of all six beams, we estimated the loss through the windows of the vacuum chamber to be $\sim 10\%$ per window. We measured the power of the trapping laser to $P_{285} \approx 15$ mW before it was split into three, and we then found a total power inside the MOT to be $P_{\text{MOT}} \approx 26$ mW. The beam size diameter was measured to $d = 5.6$ mm and we obtain the intensity inside the MOT to be $I \approx 1$ kW/m².

With $I_{\text{sat}} = 4.52$ kW/m², $\Gamma = 2\pi\nu_0 \sim 2\pi \cdot 80$ MHz and $\Delta = 2\pi \cdot 130$ MHz we obtain $\Delta\nu_{\text{Stark}} = \Delta\nu_{\text{Stark}}/2\pi \approx 1.4 \pm 0.3$ MHz. We have determined the uncertainty on $\Delta\nu_{\text{Stark}}$ from estimating the uncertainty of the power to be $\sim 25\%$. This estimation is based on our approximation of P_{MOT} and on the power-meter yielding an absolute value but being hard to calibrate to less than $\sim 20\%$.

The calculated ac Stark shift overlap with the measured value. This greatly indicates that it was the ac Stark shift we measured as expected.

4 Discussion

In the preceding sections we have characterized different aspects of the Mg $^3P_1 \leftrightarrow ^1S_0$ atomic clock. Starting with the laser system we measured the build-up intensity of the

reference cavity to obtain its line width, $\delta\nu_c$ used in the PDH setup. After fitting and calculating the weighted average of our measurements, we obtained results for $\delta\nu_c$. However, uncertainties due to problems in triggering the signal and defining the starting time occurred. With more time on hand we would have made an effort reducing these uncertainties. $\delta\nu_c$ was used in further data analysis and thus this uncertainty was included in all further calculations in section 2.

With this result on hand, we move on to the results obtained for the 914 nm master laser. In section 2.2 the (FWHM) line width of our master laser was determined by use of the Pound-Drever-Hall laser stabilization technique. One way to perform an analysis of the error signal was to perform a fast Fourier transform on the error signal. This was not possible due to lack of equipment and we used an alternative analyzing method.

By making a linear approximation of the D -coefficient and projecting the distribution of the error signal onto this linear approximation, we obtained a line width for the master laser with uncertainties corresponding to the uncertainty of the reference cavity line width and our approximations. The obtained master laser line width is an upper limit as the error signal consists of the signal from the cavity reflection and from electronic noise in the measurement devices.

The most preferable way of measuring the master laser line width would be to have two identical master lasers beating against each other. We only had one, so to obtain another result for the master laser line width for comparing, we analyzed the reflected amplitude noise signal from the reference cavity instead. This was done in section 2.3

The two results for the master laser line width differ by almost a factor 2. The reasons could be several. The line width of the master laser can fluctuate up to ~ 1 kHz due to residual effects, the success of alignment that particular day and temporal material variations [1, pp. 115]. Furthermore, the Gaussian noise, cf. Fig. 9, was approximated with a delta Dirac function and $\delta\nu_L$ is thus most likely overestimated.

In section 3.2 spectroscopy of the $^3P_1 \leftrightarrow ^1S_0$ clock transition was performed and the transmission line width was investigated. By these measurements a line width in the megahertz region was revealed and the Doppler broadening dominated the line width. Calculations of the temperature revealed a higher temperature than expected. This could indicate that other broadenings in the megahertz region were present, but it is most likely that the temperature was high due to the environment of the experiment.

The spectroscopy also revealed some unanswered questions, since it revealed two peaks instead of one. This can be caused by two different velocity components for the 3P_1 excited magnesium atoms in the MOT and would then result in a Doppler shift of the transition frequency. Two different velocity components could be induced by reflections of the clock laser and asymmetric alignments.

From the magnitude of the Doppler broadening compared to the other contributions

to the line width it is clear that the Doppler effect should be reduced for reaching higher precision for the atomic clock. By using the ac Stark effect an optical lattice can be constructed to reduce the Doppler broadening.

For the ac Stark shift we only made three measurements and in spite of this, the magnitude of the calculated and the measured values of this ac Stark shift are very similar and the ratio between these values is $\Delta\nu_{\text{calc}}/\Delta\nu_{\text{meas}} = 0.7$. This is a very satisfactory result, considering the calculation depends on an approximated value of the intensity inside the MOT. If we approximate the power to be 6 mW greater the result will be inside the uncertainty limit of our measurements. Our main achievement here is that we *did measure* the ac Stark shift and not just some deviation from the non-shifted values due to poor statistics of the measurement.

4.1 The future

After analyzing the line width of the clock transition in section 3.2 to 3.3.1 it is clear that a great reduction of the Doppler broadening is necessary to reach higher precision with the ^{24}Mg clock.

The laser lab group at NBI is, as this thesis is handed in, preparing a setup of an 1D optical lattice to eliminate the Doppler broadening and improve their atomic clock to an accuracy of 10^{-14} to 10^{-13} , maybe even to 10^{-15} by a 2D optical lattice. For the clock transition described in this thesis the success for the group depends on the magic wavelength to be found at the theoretically predicted value ~ 466 nm [21].

To trap the atoms in the optical lattice the magnesium atoms have to be cooled to at least $T \sim 1$ mK. Once the atoms are trapped in this harmonic potential the Doppler effect and recoil motion is eliminated as mentioned in section 3.4. This reduces the clock transitions line width greatly, going from a value ~ 10 MHz to ~ 10 kHz from the power broadening, cf. Eq. 18. Hence improving the clock accuracy.

To increase the atoms lifetime inside the MOT, they can be tightly bound in the optical lattice by the side-band cooling technique. Right after trapping in the harmonic potential they will be distributed around the $n_z \approx 30$ level of the harmonic potential. For an atom sitting in the n th level of the ground state, $^1\text{S}_0$, the clock laser can be used to excite it to the $n_z - 1$ level of the $^3\text{P}_1$ state. The strongest transition is for $\Delta n_z = 0$ [7]. This makes the atom drop back to the $n_z - 1$ level of the ground state. Exciting the atoms in this manner an appropriate number of times, the distribution of the atoms can be brought down from having a mean value of $n_z \approx 30$ to $n_z \approx 1$. Hence effectively cooled down to a temperature $T \sim 1$ μK [3].

5 Conclusion

In this thesis we have characterized some of the main properties of the ^{24}Mg atomic clock.

In section 2 we measured the line width of the 914 nm master laser by two different methods. We found $\delta\nu_L = 1.2 \pm 0.2$ kHz from the PDH error signal and $\delta\nu_L = 2.2 \pm 0.2$ kHz from analyzing the amplitude noise of the reflected signal from the reference cavity in the PDH setup.

In section 3 we measured the line width of the $^{24}\text{Mg } ^3\text{P}_1 \leftrightarrow ^1\text{S}_0$ clock transition and found it to be greatly dominated by the Doppler broadening since $\delta\nu_{cl} = 11.24 \pm 0.28$ MHz and $\delta\nu_{cl} = 12.28 \pm 0.32$ MHz. From this result we calculated the temperature inside the MOT to be in the range: 14.5 to 16.6 mK. in section 3.3.1. Finally we measured and calculated the ac Stark shift of the clock transition, when perturbed by the 285 nm trapping laser, to $\Delta\nu_{\text{Stark}} = 1.96 \pm 0.27$ MHz and $\Delta\nu_{\text{Stark}} \approx 1.4 \pm 0.3$ MHz respectively.

References

- [1] F. Riehle, Frequency Standards: Basics and Applications. Wiley-VCH, 2004.
- [2] A. D. Ludlow, T. Zelevinsky, G. K. Campbell, S. Blatt, M. M. Boyd, M. H. G. de Miranda, M. J. Martin, J. W. Thomsen, S. M. Foreman, J. Ye, T. M. Fortier, J. E. Stalnaker, S. A. Diddams, Y. Le Coq, Z. W. Barber, N. Poli, N. D. Lemke, K. M. Beck, and C. W. Oates, “Sr lattice clock at 1×10^{-16} fractional uncertainty by remote optical evaluation with a ca clock,” Science, vol. 319, pp. 1805–1808, 3 2008.
- [3] S. Blatt, A. D. Ludlow, G. K. Campbell, J. W. Thomsen, T. Zelevinsky, M. M. Boyd, J. Ye, X. Baillard, M. FouchÈ, R. Le Targat, A. Brusch, P. Lemonde, M. Takamoto, F. L. Hong, H. Katori, and V. V. Flambaum, “New limits on coupling of fundamental constants to gravity using sr87 optical lattice clocks,” Physical Review Letters, vol. 100, 04 2008.
- [4] J. J. Sakurai, Modern Quantum Mechanics. Addison Wesley Longman, revised ed., 1994.
- [5] H. S. Margolis, “Frequency metrology and clocks,” Journal of Physics B: Atomic, Molecular and Optical Physics, vol. 42, no. 15, p. 154017, 2009.
- [6] J. R. Taylor, An Introduction to Error Analysis: The Study of Uncertainties in Physical Measurements. University Science Books, U.S., 2nd ed., 1997.
- [7] M. M. Boyd, High Precision Spectroscopy of Strontium in an Optical Lattice: Towards a New Standard for Frequency and Time. PhD thesis, University of Colorado, 2007.

-
- [8] T. Udem, S. A. Diddams, K. R. Vogel, C. W. Oates, E. A. Curtis, W. D. Lee, W. M. Itano, R. E. Drullinger, J. C. Bergquist, and L. Hollberg, “Absolute frequency measurements of the hg+ and ca optical clock transitions with a femtosecond laser,” Physical Review Letters, vol. 86, 05 2001.
- [9] Quantum-mechanical theory of optical coherence. Kungl. Vetenskapsakademien, October 2005. Advanced information on the Nobel Prize in Physics 2005.
- [10] C. J. Foot, Atomic Physics. Oxford University Press, 2005.
- [11] P. W. Milonni and J. H. Eberly, Lasers. Wiley-Interscience, 1988.
- [12] V. Ruseva, Design of high-power frequency-doubled diode laser systems for experiments on laser-cooled Magnesium. PhD thesis, The Niels Bohr Institute, University of Copenhagen, 2005.
- [13] Y. Gong and B. Li, “High-reflectivity measurement with a broadband diode laser based cavity ring-down technique,” Applied Physics B: Lasers and Optics, vol. 88, pp. 477–482, 08 2007.
- [14] E. D. Black, “An introduction to pound–drever–hall laser frequency stabilization,” American Journal of Physics, vol. 69, no. 1, pp. 79–87, 2001.
- [15] B. B. Jensen, Production and Interrogation of Metastable Magnesium Atoms: Towards an Atomic Clock. PhD thesis, The Niels Bohr Institute, University of Copenhagen, 2009.
- [16] H. Katori, M. Takamoto, V. G. Pal’chikov, and V. D. Ovsiannikov, “Ultrastable optical clock with neutral atoms in an engineered light shift trap,” Physical Review Letters, vol. 91, 10 2003.
- [17] J. Ye, H. J. Kimble, and H. Katori, “Quantum State Engineering and Precision Metrology Using State-Insensitive Light Traps,” Science, vol. 320, no. 5884, pp. 1734–1738, 2008.
- [18] C. C. Gerry and P. L. Knight, Introductory Quantum Optics. Cambridge University Press, 3rd ed., 2008.
- [19] N. Lundblad, M. Schlosser, and J. V. Porto, “Experimental observation of magic-wavelength behavior of Rb-87 atoms in an optical lattice,” Physical Review A, vol. 81, MAR 2010.
- [20] P. Rosenbusch, S. Ghezali, V. A. Dzuba, V. V. Flambaum, K. Beloy, and A. Derevianko, “ac Stark shift of the Cs microwave atomic clock transitions,” Physical Review A, vol. 79, JAN 2009.

-
- [21] A. Derevianko, B. Obreshkov, and V. A. Dzuba, “Mapping out atom-wall interaction with atomic clocks,” Physical Review Letters, vol. 103, 09 2009.